indicates $\Delta H°$ is 144 kJ/mol for reaction 3, quite close to our calculated value of 169 kJ/mol for the gas-phase reaction 2. They find, furthermore, a value of 139 J/deg·mol for $\Delta S°$.

Conclusion

Using molecular orbital theory, we have determined reaction mechanisms for sodium sulfate and sodium pyrosulfate formation from solid sodium chloride, sulfur dioxide, and oxygen. The reaction involves a singlet $SO_2 \cdot O_2$ intermediate adsorbed to the NaCl surface. Gas-phase SO_3 abstracts an oxygen atom from O_2 in the $SO_2 \cdot O_2$ adduct, forming SO_4^{2-}. As this anion forms Na^+ cations from the surface bond to it and $Cl_2(g)$ desorbs. The anion has two pathways open to it; the lower-energy one has it bonding to the SO_3 left behind on the surface, forming $S_2O_7^{2-}$. Both the sulfate and pyrosulfate precursors undergo low-energy umbrella distortions leading to tetrahedral sulfur coordination. Though pyrosulfate is more stable at low temperature, at high temperature it is driven by entropy to lose SO_3, yielding sodium sulfate.

Acknowledgment. We are warmly appreciative to Drs. William L. Fielder, Fred J. Kohl, and Carl A. Stearns of the NASA Lewis Research Center for advice concerning this work, which has been supported by NASA Grant NAG3-341.

Registry No. $Na_2S_2O_7$, 13870-29-6; NaCl, 7647-14-5; SO_2, 7446-09-5; O_2, 7782-44-7; SO_3, 7446-11-9.

(13) L. P. Kostin, L. L. Pluzhnikov, and A. N. Ketov, *Russ. J. Phys. chem.*, **49**, 2235 (1975).

Theoretical Study of the Triple Metal Bond in d^3-d^3 Binuclear Complexes of Chromium, Molybdenum, and Tungsten by the Hartree-Fock-Slater Transition State Method

Tom Ziegler

Contribution from the Department of Chemistry, University of Calgary, Calgary, Alberta, Canada T2N 1N4. *Received April 25, 1983*

Abstract: Hartree-Fock-Slater calculations are reported for the two metal fragments MoL_3 and CrL_3 with L = H, CH_3, Cl, NH_2, and OH. The ML_3 systems all have a trigonal planar geometry with the metal-to-ligand bond strength in the order OH > Cl > NH_2 > CH_3 > H. The bonding energies of MoL_3 are somewhat larger than the corresponding energies of CrL_3. Hartree-Fock-Slater calculations are also reported for the two binuclear systems Mo_2L_6 and Cr_2L_6 with L = H, CH_3, Cl, NH_2, and OH. The staggered conformation is the preferred geometry for all the systems. The optimized metal-metal bond distances are calculated to be in the range 2.22 to 2.25 Å for the Mo systems and in the range 1.91 to 1.95 Å for the Cr systems. The strength of the metal-metal bonds follows the order Mo-Mo (468-414 kJ mol^{-1}) > Cr-C (301-217 kJ mol^{-1}). A study of W_2H_6 showed that the inclusion of relativistic effects increased the metal-metal bond energy from 422 to 535 kJ mol^{-1}.

1. Introduction

There has recently been considerable interest in the electronic structure of binuclear d^3-d^3 complexes following the synthesis and structural characterization of several M_2L_6 systems[1] with M = Mo and W.

A qualitative outline of the bonding in M_2L_6 was first given by Albright and Hoffmann.[2] The authors suggested that the observed staggered conformation of M_2L_6 is due to steric repulsions between ligands on different metal centers. It was proposed that the eclipsed conformation, favored by electronic factors according to ref 2, would be adopted by M_2L_6 for small-size ligands.

It has recently been possible to carry out ab initio calculations on binuclear metal compounds. Kok and Hall[3] have, in connection with a previous work, published results from ab initio calculations on Mo_2H_6 and $Mo_2(NH_2)_6$. They calculated the Mo-Mo bond strength D(Mo≡Mo) in Mo_2H_6 to be 118 kJ mol^{-1} and suggested, based on an error analysis, that a more extensive treatment (larger size configuration interaction) would give D(Mo≡Mo) as 248 kJ mol^{-1}. Tentative calculations on $Mo_2(NH_2)_6$ indicated that the replacement of L = H with L = NH_2 might increase D(Mo≡Mo) further by 117 kJ mol^{-1}. The best experimental determination[4] of D(Mo≡Mo), due to Adedeji et al.,[4] gives D(Mo≡Mo) as 398 kJ mol^{-1}. However, the experimental determination of D(Mo≡Mo) is somewhat hampered by uncertainties in the energy assigned to the Mo-L bonds.

Transition metal complexes have been studied extensively by the HFS method first suggested by Slater.[5] One of the most popular implementations of the HFS scheme is the Xα-SW method due to Johnson.[6]

Bursten, Cotton et al.[7] have recently published Xα-SW calculations on $Mo_2(NH_2)_6$, $Mo(N(CH_3)_2)_6$, $Mo_2(OH)_6$, and $Mo_2(CH_3)_6$. They provide a sophisticated analysis of the valence orbitals along with a correlation of calculated and experimental ionization potentials. Bursten et al.[7] dispute that the preferred geometry of M_2L_6 for small ligands should be eclipsed. They suggest that electronic factors would prefer a geometry for M_2L_6 for the two ML_3 fragments in a planar trigonal conformation and a free rotation around the metal-metal bond.

The Xα-SW scheme cannot calculate the total electronic energy accurately owing to an approximate representation of the molecular electronic potential. It is for this reason not possible to optimize molecular geometries or calculate bonding energies with the Xα-SW method.

We have used another implementation of the HFS method, due to Baerends et al.,[8] in which the molecular electronic potential

(1) (a) Cotton, F. A. *Acc. Chem. Res.* **1978**, *11*, 225. (b) Chrisholm, M. H.; Cotton, F. A. *Ibid.* **1978**, *11*, 356.
(2) Albright, T. A.; Hoffmann, R. *J. Am. Chem. Soc.* **1978**, *100*, 7736.
(3) Kok, R. A.; Hall, M. B. *Inorg. Chem.* **1983**, *22*, 728.
(4) Adedeji, F. A.; Cavell, K. J.; Cavell, S.; Connor, J. A.; Pilcher, G.; Skinner, H. A.; Safarani-Moattar, M. T. *J. Chem. Soc., Faraday Trans. 1* **1979**, *75*, 603.
(5) Slater, J. C. *Adv. Quantum Chem.* **1972**, *6*, 1.
(6) Johnson, K. H. *J. Chem. Phys.* **1966**, *45*, 3085.
(7) Bursten, B. E.; Cotton, F. A.; Green, J. C.; Seddon, E. A.; Stanley, G. G. *J. Am. Chem. Soc.* **1980**, *102*, 4579.
(8) (a) Baerends, E. J.; Ellis, D. E.; Ros, P. *Chem. Phys.* **1976**, *2*, 41. (b) Baerends, E. J.; Ros, P. *Int. J. Quantum Chem.* **1978**, *S12*, 169.

0002-7863/83/1505-7543$01.50/0

is represented accurately. This scheme in connection with the generalized transition state method[9] has been shown to provide reliable geometrical parameters and bonding energies. Snijders et al.[10] have recently extended the method by Baerends et al. to include relativistic effects.

The first part of this study explores the potential surface of the MoL_3 and CrL_3 fragments, along with the stability of the M–L bond, for a number of different ligands, L = H, CH_3, Cl, NH_2, and OH.

The ML_3 fragments are combined in the second part to form Mo_2L_6 as well as the unknown homologous Cr_2L_6 system. A discussion is given of the preferred conformation and the metal–metal bond strength as a function of the electronic and steric factors, as well as the different ligands.

We have previously analyzed the importance of relativistic effects on the metal–metal bond strength in Au_2 and Hg_2^{2+}.[11] This discussion will be extended to W_2L_6 represented by W_2H_6. It is shown that relativistic effects strengthen the metal–metal bond in W_2H_6 to the extent where $D(W{\equiv}W) > D(Mo{\equiv}Mo)$.

2. Computational Details

2.1 The Method. The many-electron wave function representing the molecular systems was restricted to a single Slater determinant. The total electronic energy was evaluated from the corresponding statistical energy expression with a standard exchange scale factor of $\alpha = 0.70$. The statistical energy expression has recently been extended[12,13] to multideterminantal wave functions so as to cover the case of a weakly bound system, for which a single Slater determinant is inadequate. Exploratory calculations on Mo_2H_6 and Cr_2H_6, based on the method in ref 12, showed that the binuclear systems are adequately represented by a single determinantal wave function at the equilibrium metal–metal distance. However, the single determinantal picture breaks down rapidly as the metal–metal bond is stretched toward dissociation, in particular for Cr_2L_6. The simple single determinantal picture has previously[9] been used to calculate triple bond energies for N_2 and CO, in fair agreement with experiment. We plan to use the method in ref 13 to study the strength of metal–metal bonds in complexes where the interaction is much weaker than in M_2L_6.

2.2 Basis and Computational Procedures. The molecular orbitals were expanded (LCAO) in terms of a basis set made up of Slater-type orbitals (STO's). The ns, np, nd, $(n+1)$s and $(n+1)$p shells on the metals as well as the ns and np shells on the ligand atoms were considered as valence, and represented by an uncontracted triple-ζ STO basis set due to Snijders et al.[14] The other shells of lower energy were taken as core and frozen according to the procedure given in ref 8. The calculation of matrix elements of the HFS one-electron Hamiltonian has been performed by numerical intergration (see ref 8 and references therein). In order to describe accurately the Coulomb and exchange potentials, extensive fits of the density were carried out using a set of fit functions including s-, p-, d-, f-, and g-type STO functions on the metal, and s-, p-, and d-type STO functions on the ligand atoms. These computational approximations lead to errors of at most 0.001 au in the orbital energies.

2.3 Geometries. The geometrical parameters not optimized in the calculations were taken from Bursten et al.[7]

$M_2(NH_2)_6$. The fixed bond distances and angles are as follows: N–H = 0.978 Å, M–N–H_1 = 116.3°, M–N–H_2 = 133.4°, and H–N–H = 110.3°. The NH_2 ligands are in the reflection planes of the ML_3 fragments. The M–M and M–M distances as well as the M–M–N angle were optimized.

$M_2(OH)_6$. The fixed distances and angles are as follows: O–H = 0.958 Å and M–O–H = 109°. The OH ligands are in the three reflection planes of ML_3. The M–M and M–O distances were optimized along with the M–M–O angle.

$M_2(CH_3)_6$. The fixed bond distances and angles are as follows: C–H = 1.00 Å, M–C–H = 115.0°. Each of the CH_3 ligands has one H atom in a reflection plane of ML_3. The M–M and M–C distances as well as M–M–C are all optimized.

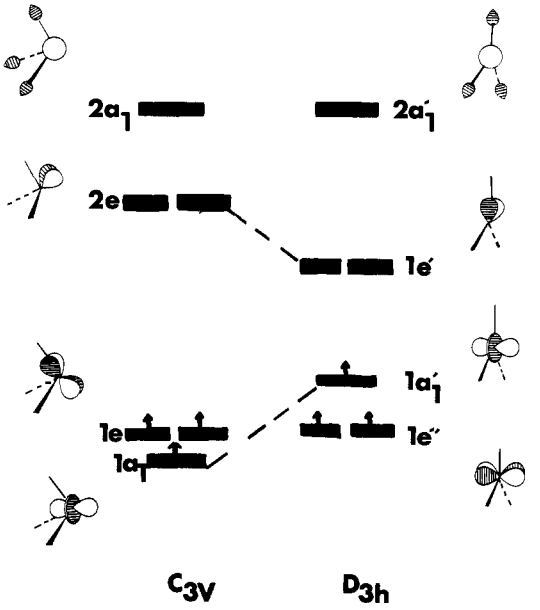

Figure 1. Schematic orbital level diagrams for the d^3 ML_3 fragment according to HFS calculations. To the left are shown the highest occupied and lowest unoccupied orbitals of ML_3 in the trivacant octahedron conformation of C_{3v} symmetry. The corresponding orbitals for the trigonal planar geometry of D_{3h} symmetry are shown to the right.

M_2H_6 and M_2Cl_6. All parameters were optimized.

The fragments $M(NH_2)_3$, $M(OH)_3$, and $M(CH_3)_3$ all have C_{3v} symmetry. The two fragments MH_3 and MCl_3 have C_{3v} symmetry except for the trigonal planar geometry, where the point group is D_{3h}. We shall use the notion of trigonal planar symmetry for $M(NH_2)_3$, $M(OH)_3$, and $M(CH_3)_3$ as well, when the three nuclei (N, O, or C) attached to the central atom are in the same plane as M.

3. ML_3 Fragment

We shall in this section discuss the metal-to-ligand bond energies in MoL_3 and CrL_3 for various ligands (L = H, Cl, CH_3, OH, NH_2) along with the electronic structure and prefered geometry of the ML_3 moiety **1** in the d^3 case.

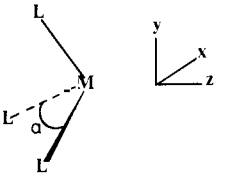

1

3.1 Electronic Structure of CrL_3 and MoL_3. A general outline of the electronic structure in ML_3 has been given previously.[15,16] The molecular orbital energy levels of ML_3 with the lowest energies correspond to nonbonding ligand orbitals or bonding ligand to metal combinations. They are all fully occupied. The upper levels, on the other hand, correspond to nonbonding metal orbitals or antibonding ligand to metal combinations. The upper levels and their associated orbitals are represented schematic in Figure 1 for two limiting shapes of ML_3; the trivacant octahedron (α = 90°) conformation **2** of C_{3v} symmetry, and the trigonal planar conformation **3** of D_{3h} symmetry.[17]

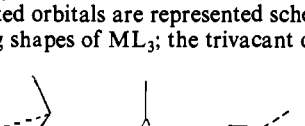

2 **3** **4**

(9) Ziegler, T.; Rauk, A. *Theor. Chim. Acta* **1977**, *46*, 1.
(10) (a) Snijders, J. G.; Baerends, E. J. *Mol. Phys.* **1978**, *36*, 1789. (b) Snijders, J. G.; Baerends, E. J.; Ros, P. *Ibid.* **1979**, *38*, 1909.
(11) Ziegler, T.; Snijders, J. G.; Baerends, E. J. *J. Chem. Phys.* **1981**, *74*, 1271.
(12) Noodleman, L. *J. Chem. Phys.* **1981**, *74*, 5737.
(13) Ziegler, T. "Functional Theory in Atoms, Solids and Molecules"; Dahl, J. P., Ed.; Plenum Press, New York, 1983.
(14) Snijders, G. J.; Baerends, E. J.; Vernooijs, P. *At. Nucl. Data Tables* **1982**, *26*, 483; and private communication.
(15) Albright, T. A.; Hoffmann, R. *J. Am. Chem. Soc.* **1977**, *99*, 7546.
(16) Ziegler, T.; Rauk, A. *Inorg. Chem.* **1979**, *18*, 1755.

Table I. Calculated Bonding Energies and Bond Distances in MoL_3 and CrL_3 for the Trigonal Planar Geometry

	CrL_3		MoL_3	
L	ΔE_{ML} (kJ mol^{-1})	R_{ML} (Å)	ΔE_{ML} (kJ mol^{-1})	R_{ML} (Å)
H	88	1.70	125	1.83
CH_3	242	2.01[a]	276	2.11[a]
NH_2	255	1.87[a]	301	1.99[a]
Cl	272	2.22	305	2.38
OH	439	1.81[a]	481	1.88[a]

[a] For polyatomic ligands R_{ML} corresponds to the distance between the metal atom and N, C, or O.

The d manifold has one pair of orbitals of zero overlap with the α-ligand combinations. This pair transforms as the e irreducible representation and represents the 1e (1e″) level of Figure 1. Another pair, also transforming as e, has a substantial overlap with the σ-ligand orbitals. This pair can thus form a bonding combination, representing one of the fully occupied levels of lower energy, as well as the antibonding combination shown in Figure 1 as 2e (1e′). The remaining d_{z^2} orbital is nonbonding with respect to the σ-ligand combinations in the trivacant conformation **2** because of symmetry and represents $1a_1$ of Figure 1. An overlap between d_{z^2} and the σ-ligand combination emerges as α is changed from 90° in **2** to 120° in **3**. The d_{z^2} orbital can thus in the trigonal planar geometry **3** form a bonding combination as well as the antibonding combination shown as $1a_1'$. The bonding character for orbitals of lower energy in ML_3 is enhanced further, somewhat depending on the ligand L, by $(n+1)$p and, in particular, $(n+1)$s. The $(n+1)$p, $(n+1)$s set forms in turn, just as with the d manifold, antibonding combinations, of which the one lowest in energy is shown as $2a_1$ ($2a_1'$) in Figure 1. The $2a_1$ ($2a_1'$) orbital is primarily of $(n+1)$s character.

The state function representing the electronic ground state of **2** has the symmetry $^4A_2$ corresponding to the configuration $(1a_1)^1(1e)^2$, whereas the symmetry designation[18] for the ground state of **3** is $^4A_2'$ with the configuration $(1a_1')^1(1e'')^2$.

3.2 Geometry and Stability of CrL_3 and MoL_3. It is of interest in connection with a discussion of the preferred equilibrium geometry for the ML_3 fragments to consider the influence of electronic as well as steric effects.

The electronic effects in the d^3 fragments would favor **2** with all three electrons in nonbonding orbitals over **3** with one electron in the antibonding $1a_1'$ orbital; see Figure 1.

The steric effects, arising from four-electron destabilizing interactions between fully occupied ligand orbitals, would, on the other hand, clearly favor **3** over **2**, since the ligand–ligand overlaps are minimized in the trigonal planar conformation **3** with the largest distance between the ligands.

HFS calculations on several ML_3 fragments with M = Mo, Cr and L = H, Cl, OH, NH_2, CH_3 all gave the preferred equilibrium geometry as **3**. The difference in energy between **3** and **2** was smallest (38 kJ mol^{-1}) for MoH_3 and largest (130 kJ mol^{-1}) for $CrCl_3$. Considerations were also give to the T-shaped conformation **4** in the case of MH_3 and MCl_3. The ML_3 fragments of geometry **4** had, as one would expect if steric effects were predominant, and energy intermediate between **2** and **3**. The T-shaped geometry was as little as 21 kJ mol^{-1} above **3** in the case of MoH_3 and as much as 94 kJ mol^{-1} above **3** in the case of $CrCl_3$. We conclude, based on our HFS calculations, that MoL_3 and CrL_3 in the d^3 case prefer the trigonal planar geometry **3** because of steric effects, even for modest-sized ligands such as H and Cl.

Yates and Pitzer[19] have carried out ab initio calculations on MF_3 systems for Sc, Ti, V, Cr, Mn, Co, and Ni. All systems were calculated to have the geometry **3**, except for CrF_3 where the F–Cr–F angle was 117°.

The calculated metal-to-ligand bonding energies as well as the optimized metal-to-ligand bond distances are given in Table I for ML_3 in the trigonal planar geometry. The ligand to metal bond energy is defined as:

$$\Delta E_{ML} = -1/3*[E(ML_3) - E(M) - 3*E(L)] \quad (1)$$

where $E(ML_3)$ is the total energy of ML_3 in the electronic ground state with symmetry[18] $^4A_2'$, and $E(M)$ the total energy of the metal corresponding to the configuration $nd^5(n+1)s^{-1}$ and the symmetry term ^7S. The total energy of the ligand L, with one unpairdd electron, is given in eq 1 as $E(L)$.

An analysis of the different contributions to ΔE_{ML}, based on the energy decomposition scheme of ref 20, showed that there are two predominant contributions to the bonding energies in MoL_3 and CrL_3. The parallel trend in the metal-to-ligand bonding energies (see Table I) with respect to the different ligands on CrL_3 and MoL_3 can be traced to an ionic contribution, where charge is transferred from (predominantly) $(n+1)$s to the ligand orbitals. The transfer of charge as well as ΔE_{ML} is largest in the case of L = OH and smallest for H = L, with L = NH_2, CH_3, and Cl as intermediate cases. This trend can roughly be rationalized by considering the difference in electron affinity among the different ligands.

The second major contribution is covalent and involves the σ-binding overlaps between σ orbitals on the ligands and (predominantly) d orbitals on the metal. The 4d orbitals of Mo have somewhat better overlaps with the ligands than the 3d orbitals of Cr. The bonding energies for MoL_3 are as a consequence somewhat larger than the corresponding bonding energies in CrL_3 (see Table I). The difference in stability between CrL_3 and MoL_3 is enhanced further by the larger steric repulsion between the ligands in CrL_3.

Experimental bonding energies are not available for systems like MoL_3 and CrL_3. For TiL_4, ZrL_4, and HfL_4 experimental[21] bonding energies are in the order OR > Cl > NR_2 > CR_3 and the 4d-metal Zr has a stronger bond to the ligands than the 3d-metal Ti. Both trends are in line with the calculated bonding energies of CrL_3 and MoL_3 (see Table I).

The actual orbitals from HFS calculations on MoL_3 and CrL_3 are only schematically represented in Figure 1. This figure as well as the qualitative discussion on the electronic strucure of ML_3 applies to a simple σ-only model, in which π overlaps are neglected. Of importance for the following discussion of the binuclear systems is the identity of the orbitals representing 1e″, 1e′ in conformation **3** and 1e, 2e in conformation **2**. The more complete HFS calculations, where π overlaps are included, do not change the character of 1e′ and 1e″ in Figure 1 as metal-based d orbitals with respectively π symmetry and δ symmetry around the threefold axis. The σ model gives 1e and 2e of **2** as d orbitals tilted away from the threefold axis (see Figure 1). The π-ligand orbitals can,[15] depending somewhat on the nature of L, change the tilt angle in the full HFS calculation. However, such modifications do not change the general picture of 1e″ in **3** as better suited for metal–metal bonding than 1e of **2**, and we shall continue to base our qualitative arguments on the simple σ model, as we discuss M_2L_6 in the next section.

4. Electronic Structure and Stability of M_2L_6

We can combine the two ML_3 fragments into a binuclear complex with a staggered conformation **5a** as well as an eclipsed conformation **5b**. The ML_3 fragment was calculated to adopt a trigonal planar geometry. In calculations on M_2L_6 this geometry will be relaxed so as to allow the two fragments to distort toward the trivacant octahedron geometry of **2**. The distortion will be described in terms of β, the angle between the threefold rotation axis along the metal–metal bond and the metal-to-ligand bond

(17) The notion of trigonal planar symmetry for $M(NH_2)_3$, $M(OH)_3$, and $M(CH_3)_3$ is explained in section 2.3.

(18) The classification of $M(NH_2)_3$, $M(OH)_3$, and $M(CH_3)_3$ in terms of D_{3h} for conformation **3** apply only to the simple σ model. The full HFS calculations were carried out in C_{3v} symmetry.

(19) Yates, J. H.; Pitzer, R. M. *J. Chem. Phys.* **1979**, *70*, 4049.

(20) Ziegler, T.; Rauk, A. *Inorg. Chem.* **1979**, *18*, 1558.

(21) Lappert, M. F.; Patil, D. S.; Pedley, J. B. *J. Chem. Soc., Chem. Commun.* **1975**, 830.

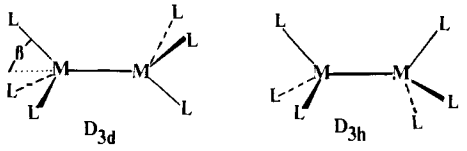

5a **5b**

vectors. We shall now discuss the strength of the metal–metal bond, as well as the relative stability of **5a** and **5b**, in terms of the angle β.

4.1 Qualitative Bonding Picture of M_2L_6. The three odd electrons on each ML_3 fragment can pair up in M_2L_6 so as to form a triple metal–metal bond. One pair will occupy the in-phase combination between $1a_1$ orbitals on the two fragments. This σ-type orbital of a_1 symmetry will have the same energy in the staggered conformation **6a** as in the eclipsed conformation **6b**.

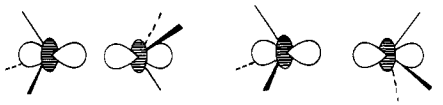

6a **6b**

The $1a_1$ orbital on each fragment is represented by a d_{z^2} orbital that is nonbonding with respect to the three ligands in the trivacant octahedron case of $\beta = 54.7°$ and slightly antibonding with respect to the ligands in the trigonal planar case of $\beta = 90°$ (see Figure 1). One would than expect the σ orbital to be somewhat more stable for $\beta = 54.7°$ as compared to $\beta = 90°$.

The remaining two electron pairs will reside in a degenerate set of orbitals constructed from bonding combinations between 1e (1e″) on the two ML_3 fragments. The two bonding orbitals will be of e_u symmetry in the staggered conformation, D_{3d}, and of e′ symmetry, D_{3h}, in the eclipsed conformation. The 1e″ orbital on ML_3, **7a**, is well suited for metal–metal bonding at $\beta = 90°$.

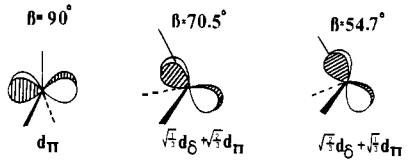

7a **7b** **7c**

The two lobes are pointing along the threefold axis and the resulting set of orbitals, **8a** of e_u symmetry and **8b** of e′ symmtery,

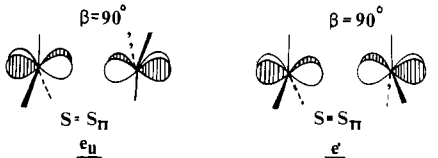

8a **8b**

can form pure metal–metal π bonds. The energies of **8a** and **8b** will be closely the same. A change of β toward 54.7° will tilt the lobes of the 1e orbital away from the threefold axis, so as to maintain a nonbonding interaction with the ligands **7b** and **7c**. The overlaps in e′, **9b**, and particularly e_u, **9a**, will as a consequence

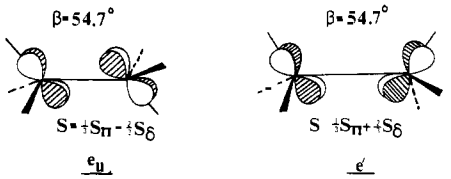

9a **9b**

be substantially reduced. The energy of **9b** will be higher than **9b**, and both will have energies higher than either **8a** or **8b**. A close examination[22] has shown that the bonding overlaps at $\beta = 54.7°$ is $^1/_3S_{d\pi} - {}^2/_3S_{d\delta}$ in e_u, **9a**, and $^1/_3S_{d\pi} + {}^2/_3S_{d\delta}$ in e′. Here $S_{d\pi}$, $S_{d\delta}$ refer to overlaps between two d orbitals of π symmetry and δ symmetry, respectively, with respect to the metal–metal axis.

The corresponding overlaps for $\beta = 70.5°$, where the LML angle is "tetrahedral", would give $^2/_3S_{d\pi\pi} - {}^1/_3S_{d\delta}$ for e_u and $^2/_3S_{d\pi} + {}^1/_3S_{d\delta}$ for e′.

The stronger bonding interaction in either **8a** or **8b**, as compared to **9a**, **9b**, points to an electronically preferred geometry in which the two ML_3 fragments both are in a trigonal planar conformation with free rotation around the metal–metal bond, as suggested by Bursten et al.[7] This arrangement is further stabilized by the preference of the free ML_3 fragments for conformation **3**.

We shall, in the text section, use the qualitative picture given here to interpret the results from HFS calculations on Mo_2L_6 and Cr_2L_6, where L = H, CH_3, Cl, NH_2, and OH.

4.2 HFS Calculations on Cr_2L_6 and Mo_2L_6. The computational results are presented in Table II for Cr_2L_6 and in Table III for Mo_2L_6. The tables display the optimized[23] angle β and the optimized metal–metal bond distance R_{MM} for conformation **5a** as well as **5b**. Also shown is the calculated metal–metal bond energy ΔE_{MM}. The metal–metal bond energy ΔE_{MM} is defined as:

$$\Delta E_{MM} = -\{E(M_2L_6) - 2E(ML_3)\} \qquad (2)$$

where $E(M_2L_6)$ is the total energy of the binuclear complex and $E(ML_3)$ the total energy of the ML_3 fragment in the trigonal planar geometry **3** corresponding to an electronic groundstate of $^4A'$ symmetry. The metal-to-ligand bond distances were taken from the optimization of R_{ML} aon the ML_3 fragments (Table I).

The staggered conformation **5a** is calculated to be more stable than the eclipsed conformation **5b** at the HFS level of sophistication for all the model systems in Tables II and Table III, with a barrier of rotation between 29 and 60 kJ mol^{-1}. The "ideal"

Table II. Optimized Geometrical Parameters and Calculated Metal-Metal Bonding Energies for Cr_2L_6

L	conformation	β^a (deg)	R_{MM} (Å)	ΔE_{MM} (kJ mol^{-1})
H	stag.	90	1.91	301
	ec.	82	1.99	251
CH_3	stag.	79	1.92	276
	ec.	74	2.01	226
Cl	stag.	75	1.92	238
	ec.	68	2.04	196
NH_2	stag.	82	1.92	259
	ec.	74	2.03	205
OH	stag.	80	1.95	276
	ec.	74	2.06	217

[a] For a definition, see text.

Table III. Optimized Geometrical Parameters and Calculated Metal-Metal Bonding Energies for Mo_2L_6

L	conformation	β^a (deg)	R_{MM} (Å)	ΔE_{MM} (kJ mol^{-1})
H	stag.	90	2.22	447
	ec.	82	2.23	418
CH_3	stag.	83	2.25	440
	ec.	77	2.27	401
Cl	stag.	78	2.24	414
	ec.	74	2.29	376
NH_2	stag.	82	2.22	468
	ec.	76	2.25	405
OH	stag.	85	2.24	426
	ec.	78	2.28	385

[a] For a definition, see text.

(22) Dedieu, A.; Albright, T. A.; Hoffmann, R. *J. Am. Chem. Soc.* **1979**, *101*, 3141.

(23) We have used the method by Murtagh, B. A.; Sargent, R. W. H. *Comput. J.* **1970**, *13*, 185, for the geometry optimizations. The energy gradient for each degree of freedom was evaluated from three energy calculations. The required cpu time for one energy calculation of M_2L_6 was 2–5 h on a Honeywell Level 68 Multics computer system.

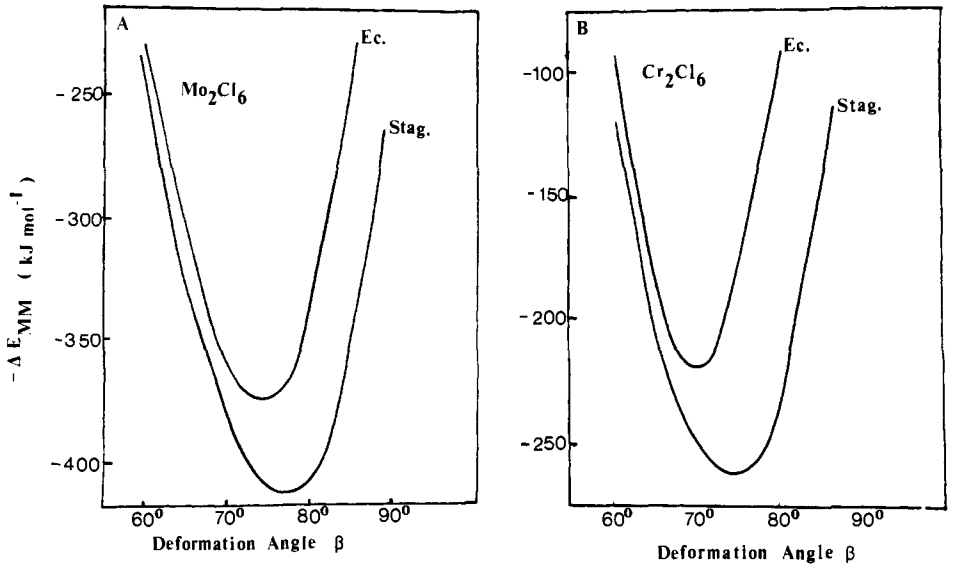

Figure 2. The change in energy of the M_2Cl_6 systems as a function of the deformation angle β for the staggered conformation (stag.) and the eclipsed conformation (ec.), respectively. The metal–metal distances for Mo_2Cl_6 in Figure 2A were 2.24 Å (stag.) and 2.29 Å (ec.). The metal–metal distances for Cr_2Cl_6 in Figure 2B were 1.98 Å (stag.) and 2.04 Å (ec.).

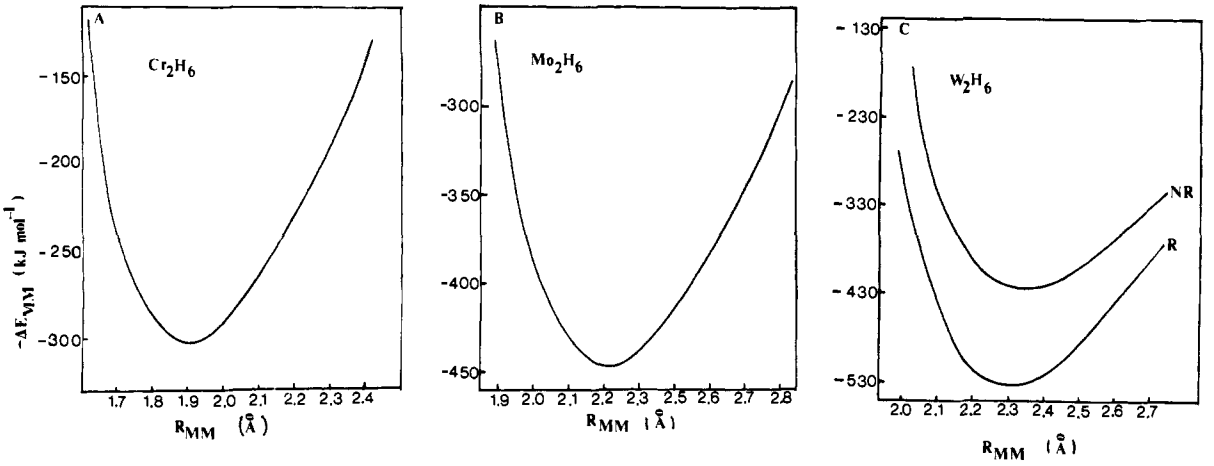

Figure 3. The variation of $-\Delta E_{MM}$ as a function of the metal–metal distances (R_{MM}) for: (a) Cr_2H_6, (b) Mo_2H_6, and (c) W_2H_6. The two potential curves for W_2H_6 correspond to a nonrelativistic calculation (NR) and a relativistic calculation (R), respectively.

geometry (β = 90°) is only adopted for the two binuclear complexes, Cr_2H_6 and Mo_2H_6, with the smallest ligand, and only in the staggered conformation. All other systems have a β angle smaller than 90°. The distortion is in particularly notable for the eclipsed conformation.

The deviation from the "ideal" geometry as well as the calculated barrier of rotation can be explained in terms of the steric interaction between ligands on different metal centers, a factor not taken into account in section 4.1. The change in $E(M_2L_6)$ as a function of β is shown for Cr_2Cl_6 in Figure 2B and for Mo_2Cl_6 in Figure 2A. It is apparent that the distortion from β = 90° is accompanied by a considerable reduction in steric repulsion, in particular, for the eclipsed conformation.

There are several known binuclear complexes with a Mo–Mo triple bond for which the structure has been determined.[1] One observes for Mo_2L_6 systems, where L = OR, NR_2, or CR_3 and R represents alkyl groups, in all instances a staggered conformation with β in the range 80 to 75°. The corresponding metal–metal bond distances are relative insensitive to the nature of L; typically $R_{MM} \sim 2.2$ Å. The observed metal bond distances are quite similar to those calculated for the model system in Table III.

It was hoped that the calculation of ΔE_{MM} for binuclear systems with different ligands would reveal a substantial and systematic variation in the strength of the metal–metal bond. The calculated bond energies for Mo_2L_6 in conformation **5a** turned out, in fact, to be rather similar. For the staggered Mo_2L_6 systems the calculated bonding energies ΔE_{MM} are between 468 and 414 lkJ mol^{-1}, in fair agreement with the experimental[4] estimate of D(Mo≡Mo) = 398 kJ mol^{-1} for $Mo_2(N(CH_3)_2)_6$. The small calculated variation in ΔE_{MM} for the staggered Mo_2L_6 systems with respect to L could not be attributed to any single factor. The rather modest influence exerted by the ligands on ΔE_{MM} is, on the other hand, attributed to the fact that the three ML_3 fragment orbitals ($1a_1$, $1e_x$, $1e_y$) involved in the triple bond all primarily are metal based.

There has so far not been any report on the synthesis of a homologous Cr_2L_6 system. The calculated metal–metal bond distances for the Cr_2L_6 model systems in Table II (~1.9 Å) correspond closely to those observed in dichromium complexes with a "supershort" quadrupole bond, and the theoretical bond energies (301–238 kJ mol^{-1}) given in Table II are all similar to the energy[24] (205 kJ mol^{-1}) assigned to the Cr–Cr quadruple bond in $Cr_2(O_2CCH_3)_4$. Thus, although Cr_2L_6 is calculated to be less stable with respect to the two ML_3 fragments than Mo_2L_6, one should not exclude the possible synthesis of Cr_2L_6 in the near future.

The variation of $-\Delta E_{MM}$ as a function of R_{MM} is shown for the staggered conformation of Cr_2H_6 and Mo_2H_6 in Figure 3A and 3B, respectively. The difference in ΔE_{MM} between Mo_2L_6 and Cr_2H_6, as well as the various contributions to the strength of the metal–metal bond, can be studied conveniently by breaking down

(24) Cavell, K. A.; Garner, C. D.; Pilcher, G.; Parkes, S. *J. Chem. Soc. Dalton Trans.* **1979**, 1714.

Table IV. Energy Decomposition of ΔE_{MM} for Cr_2H_6, Mo_2H_6, and W_2H_6

compound	conformation	β (deg)	R_{MM} (Å)	ΔE^{0a}	$\Delta E_\sigma{}^a$	$\Delta E_\pi{}^a$	$\Delta E_{MM}{}^a$
Cr_2H_6	stag.	90	1.91	461.8	−314.5	−447.9	300.6
Mo_2H_6	stag.	90	2.22	374.5	−334.1	−487.5	447.1
Mo_2H_6	ec.	90	2.22	426.2	−332.9	−486.1	392.8
Mo_2H_6	ec.	82	2.23	398.3	−331.2	−485.3	418.2
W_2H_6	stag.	90	2.36	353.2	−306.3	−469.1	422.2

[a] In kJ mol^{-1}.

ΔE_{MM} into components representing the steric interaction, the σ-bonding interaction, as well as the π-bonding interaction. The decomposition can be visualized by considering the formation of M_2L_6 from ML_3 in two steps.

The two ML_3 fragments are brought together in the first step to take up their positions in M_2L_6. The electrons are confined, however, to the orbitals they occupy in the separate fragments. In the first step three electrons of spin up will occupy $1a_1$, $1e_x$, $1e_y$ on one fragment and three electrons of spin down $1a_1$, $1e_x$, $1e_y$ on the other fragment. The total wave function for this system is given by:

$$\Psi^0 = |1a_1(1)\alpha(1)1e_x(2)\alpha(2)1e_y(3)\alpha(3)\text{-}1a_1(4)\beta(4)1e_x(5)\beta(5)1e_y(6)\beta(6)| \quad (3)$$

and the corresponding energy as E^0. The steric energy is then defined by:

$$\Delta E^0 = E^0 - 2E(ML_3) \quad (4)$$

Each unpaired electron, confined to orbitals of either a_1 symmetry or e symmetry on one of the fragments, is allowed in the second step to occupy one of the three bonding molecular orbitals, **6a** or **6b** of a_1 symmetry and **9a** or **9b** of e symmetry. The energy associated with the change in the a_1 representation is defined as the σ-bonding interaction energy ΔE_σ, and the corresponding change in energy from the e representation as the π-bonding interaction ΔE_π. We have for the total bonding energy:

$$\Delta E_{MM} = -\Delta E^0 - \Delta E_\sigma - \Delta E_\pi \quad (5)$$

A more detailed account of the decomposition scheme is given in ref 20.

The variation of the three energy components as a function of R_{MM} is shown in Figure 4 for the staggered Cr_2H_6 system. The variation of each term with respect to R_{MM} is typically much larger than the corresponding variation of the sum, $-\Delta E_{MM}$.

The steric part ΔE^0 is destabilizing owing to the repulsive interactions between occupied orbitals on the two metal centers (core–core repulsion etc.) with a smaller contribution from the steric interactions between ligands on different ML_3 fragments. It is clear from Figure 4 that both the σ-bonding interaction ΔE_σ and the σ-bonding interaction ΔE_π contribute to the stability of the metal–metal bond in Cr_2H_6. The relative importance of ΔE_σ and ΔE_π depends on the metal–metal bond distance R_{MM}. At the calculated equilibrium distance one finds $-\Delta E_\sigma > -^1/_2\Delta E_\pi$, indicating that the σ bond is somewhat stronger than each of the two π bonds.

The corresponding energy terms for the staggered Mo_2H_6 system at the calculated equilibrium distance are shown in Table IV for comparison with Cr_2H_6. The steric interaction ΔE^0 is considered less repulsive and the bonding interactions ΔE_σ ΔE_π are somewhat more stabilizing in Mo_2H_6 compared to Cr_2H_6 (see Table IV). The 4d orbitals in Mo_2H_6 apparently have good bonding overlaps at a distance where ΔE^0 still is modest, whereas the more contracted 3d orbitals in Cr_2H_6 require the two Cr atoms to move close together at the expense of a considerable steric repulsion. The net result is a stronger metal–metal bond in Mo_2H_6 compared to Cr_2H_6.

Also shown in Table IV is the decomposition of ΔE_{MM} for the eclipsed conformation of Mo_2H_6. It follows from Table IV, as already stated previously, that the eclipsed conformation **5b** is higher in energy because of steric factors.

4.3 Relatiistic HFS Calculations on W_2H_6. It has been shown in a previous study[11] on Au_2 and $Hg_2{}^{2+}$ that relativistic effects have a considerable influence on the bond between two 5d metals.

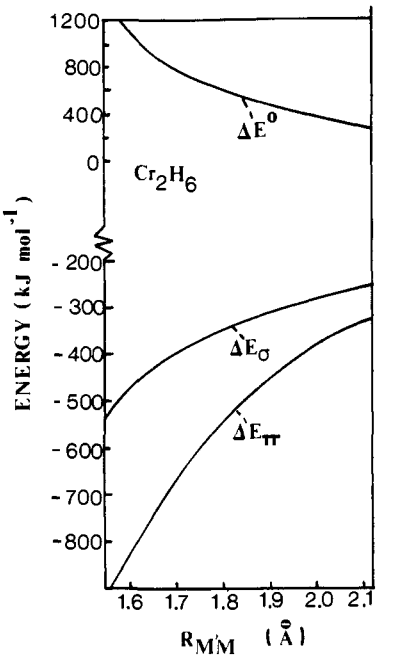

Figure 4. Decomposition of the metal–metal bonding energy ΔE_{MM} into steric interaction (ΔE^0), σ-bonding energy (ΔE_σ), and π-bonding interaction energy (ΔE_π), as a function of the metal–metal bond distance R_{MM}.

The study in ref 11 was based on the relativistic HFS method due to Snijders et al.[10] Relativity is introduced in this method to first order in α^2, where α is the fine-structure constant, through the Hamiltonian:

$$\mathcal{H}^1 = \alpha^2 H_{MV} + \alpha^2{}_{DW} + \alpha^2 H_{SO} \quad (6)$$

Here H_{MV} is the mass–velocity term, H_{DW} the Darwin term, and H_{SO} the spin–orbit term. The form of the three terms in eq 6 is discussed in ref 11.

We shall in this section extend the study of M_2L_6 from Cr_2L_6 and Mo_2L_6 to W_2L_6, through a relativistic calculation on W_2H_6. The calculated metal–metal bond energy ΔE_{MM} corresponding to W_2H_6 is shown in Figure 3C as function of the metal–metal distance R_{MM}, in the nonrelativistic case (NR) as well as the relativistic case (R). It is clear from Figure 3C that relativistic effects have a dramatic influence on the stability of the W–W bond in W_2H_6. In fact, without $\mathcal{H}^1$ the W–W bond energy would be weaker than the Mo–Mo bond in Mo_2H_6, 422 kJ mol^{-1} as compared to 447 kJ mol^{-1}. The relativistic effects stabilize the W–W bond energy to 535 kJ mol^{-1}, thus making W_2H_6 more stable than Cr_2H_6 and Mo_2H_6 with respect to the two MH_3 fragments. The calculated stronger metal–metal bond in W_2H_6 as compared to Mo_2H_6 is in line with experimental observations. Adedeji et al.[4] give $D(W{\equiv}W)$ = 558 kJ mol^{-1} and $D(Mo{\equiv}Mo)$ = 398 kJ mol^{-1} respectively for the $M_2(N(CH_3)_2)_6$ systems.

It is also worth mentioning that reltivity contracts the W–W bond from 2.36 Å in the nonrelativistic calculation to 2.31 Å in the relativistic case. The observed W–W distances in W_2L_2 are in the range 2.26 to 2.29 Å.

The main contribution to the contraction and stabilization of the W–W bond comes from the mass–velocity term H_{MV}, a

first-order relativistic correction to the kinetic energy. The mass–velocity term will, as explained in ref 11, reduce the electronic kinetic energy to an increasing extent as the two W atoms approach each other. The net effect is a lowering in the total electronic energy and a shortening of the metal–metal bond. Relativistic calculations were not carried out for the Cr_2L_6 and Mo_2L_6 systems. We expect from previous experience[11] the influence to be neglibible for Cr_2L_6, and amount to an increase of ΔE_{MM} by a few kJ mol^{-1} in the case of Mo_2L_6.

Acknowledgment. This investigation was supported by Natural Sciences and Engineering Research Council of Canada (NSERC).

Registry No. CrH_3, 87698-70-2; $Cr(CH_3)_3$, 3047-87-8; $Cr(NH_2)_3$, 20253-28-5; $CrCl_3$, 10025-73-7; $Cr(OH)_3$, 1308-14-1; MoH_3, 87698-71-3; $Mo(CH_3)_3$, 87698-72-4; $Mo(NH_2)_3$, 87698-73-5; $MoCl_3$, 13478-18-7; $Mo(OH)_3$, 60414-57-5; Cr_2H_6, 87698-74-6; $Cr_2(CH_3)_6$, 87698-75-7; Cr_2Cl_6, 87698-76-8; $Cr_2(NH_2)_6$, 87698-77-9; $Cr_2(OH)_6$, 87698-78-0; Mo_2H_6, 83636-49-1; $Mo_2(CH_3)_6$, 73581-14-3; Mo_2Cl_6, 87698-79-1; $Mo_2(NH_2)_6$, 87711-09-9; $Mo_2(OH)_6$, 64438-94-4; W_2H_6, 87698-80-4.

Anion Coordination Chemistry. ^{35}Cl NMR Studies of Chloride Anion Cryptates

Jean-Pierre Kintzinger,*[1] Jean-Marie Lehn,*[1] Elizabeth Kauffmann,*[1,2] James L. Dye,*[2] and Alexander I. Popov*[2]

Contribution from the Institut Le Bel, Université Louis Pasteur, F 67008 Strasbourg, France, and the Department of Chemistry, Michigan State University, East Lansing, Michigan 48824.
Received May 9, 1983

Abstract: The chlorine NMR signals of the chloride inclusion complexes $[Cl^- \subset L\text{-}H_n^{n+}]$, L = **1–5**, formed by the protonated species of cryptands have been measured. In combination with proton and carbon-13 NMR data, they provide information about chloride chemical shifts, mono- and bimolecular exchange processes, and quadrupolar coupling constants χ of the chloride cryptates. Very large chemical shifts are induced by cryptate formation. The high χ values calculated indicate that appreciable field gradients are generated by the ligands at the nucleus of the bound spherical anion, due to deformation of the coordination shell from ideal symmetry. The results obtained emphasize the contribution of NMR studies of anion cryptates to the field of anion coordination chemistry.

Whereas macrocyclic complexes of cations have been the subject of intense investigation over the past decade, anion coordination chemistry, the binding of anions by organic ligands, in particular of the macrocyclic type, has only recently been recognized and developed as a new area of coordination chemistry.[3,4]

Thus, macrocyclic, macrobicyclic, and macrotricyclic polyammonium and polyguanidinium receptor molecules have been shown to complex a variety of inorganic and biological anions.[3–13]

As in the case of cation complexes, physicochemical investigations should provide insight into the structure of such anion complexes and the properties of the bound anion. In this respect, direct observation of the bound species as well as of the ligand by heteronuclear NMR is a particularly powerful tool, as witnessed by numerous studies of macrocyclic cation complexes, such as alkali cryptates.[14,15]

The present work represents the first such investigation of well-defined anion complexes, the chloride cryptates of the spherical macrotricycles SC-24 (**1**), SC-25 (**2**), and SC-26 (**3**),[16] the bis(tren)macrobicycle (**4**), and the macrobicyclic diamine (**5**)[5], using ^1H, ^{13}C, ^{35}Cl, and ^{37}Cl NMR. The tetraprotonated forms of **1–3**, the hexaprotonated form of **4**, and the diprotonated form of **5** have been shown to bind various anions[4,5,17] in particular chloride, yielding chloride cryptates in which the substrate is located inside the intramolecular cavity and held by an array of zwitterionic hydrogen bonds, as represented schematically by structures **6** and **7** and confirmed by the crystal structures of these $(Cl^- \subset \mathbf{1}\text{-}4H^+)$[18] and $(Cl^- \subset \mathbf{4}\text{-}6H^+)$[19] cryptates. In the katapinates of macrobicyclic diammonium ions the anion is bound by

(1) Institut Le Bel, ERA N° 265 of the CNRS.
(2) Michigan State University.
(3) Lehn, J. M. *Pure Appl. Chem.* **1978**, *50*, 871–892.
(4) Park, C. H.; Simmons, H. E. *J. Am. Chem. Soc.* **1968**, *90*, 2431–2432. Bell, R. A.; Christoph, G. G.; Fronzeck, F. R.; Marsh, R. E. *Science* **1975**, *98*, 5727–5728.
(5) Graf, E.; Lehn, J. M. *J. Am. Chem. Soc.* **1976**, *98*, 6403–6405.
(6) Schmidtchen, F. P. *Angew. Chem.* **1977**, *89*, 751–752; *Angew. Chem., Int. Ed. Engl.* **1977**, *16*, 720–721; *Angew. Chem.* **1980**, *93*, 469–470; *Angew. Chem., Int. Ed. Engl.* **1981**, *20*, 466–468; *Chem. Ber.* **1981**, *114*, 597–607.
(7) Lehn, J. M.; Sonveaux, E.; Willard, A. K. *J. Am. Chem. Soc.* **1978**, *100*, 4914–4916.
(8) Tabushi, I.; Kuroda, Y.; Kimura, Y. *Tetrahedron Lett.* **1976**, 3327–3330.
(9) Dietrich, B.; Hosseini, M. W.; Lehn, J. M.; Sessions, R. B. *J. Am. Chem. Soc.* **1981**, *103*, 1282–1283. Peter, F.; Gross, M.; Hosseini, M. W.; Lehn, J. M.; Sessions, R. B. *J. Chem. Soc., Chem. Commun.* **1981**, 1067–1069.
(10) Kimura, E.; Sakonaka, A.; Yatsunami, T.; Kodama, M. *J. Am. Chem. Soc.* **1981**, *103*, 3041–3045. Kimura, E.; Kodama, M.; Yatsunami, T. *Ibid.* **1982**, *104*, 3182–3187.
(11) Margulis, T. N.; Zompa, L. J. *Acta Crystallogr., Sect. B* **1981**, *B37*, 1426–1428. Cullinane, J.; Gelb, R. I.; Margulis, T. N.; Zompa, L. J. *J. Am. Chem. Soc.* **1982**, *104*, 3048–3053.
(12) Hosseini, M. W.; Lehn, J. M. *J. Am. Chem. Soc.* **1982**, *104*, 3525–3527.
(13) Dietrich, B.; Fyles, T. M.; Lehn, J. M.; Pease, L. G.; Gyles, D. L. *J. Chem. Soc., Chem. Commun.* **1978**, 935–936.
(14) Popov, A. I.; Lehn, J. M. In "Coordination Chemistry of Macrocyclic Compounds"; Melson, G. A., Ed.; Plenum Press: New York, 1979; Chapter 9.
(15) Kintzinger, J. P.; Lehn, J. M. *J. Am. Chem. Soc.* **1974**, *96*, 3313–3314.
(16) Graf, E.; Lehn, J. M. *J. Am. Chem. Soc.* **1976**, *98*, 6403–6405. Graf, E.; Lehn, J. M. *Helv. Chim. Acta* **1981**, *64*, 1040–1057.
(17) Lehn, J. M.; Pine, S. H.; Watanabe, E. I.; Willard, A. K. *J. Am. Chem. Soc.* **1977**, *99*, 6766–6768.
(18) Metz, B.; Rosalky, J. M.; Weiss, R. *J. Chem. Soc., Chem. Commun.* **1976**, 533–534.
(19) Dietrich, B.; Guilhem, J.; Lehn, J. M.; Pascard, C.; Sonveaux, E., manuscript in preparation.

0002-7863/83/1505-7549$01.50/0